Compact, High-Speed and Power-Efficient Electrooptic Plasmonic Modulators

ARTICLE *in* NANO LETTERS · OCTOBER 2009

Impact Factor: 13.59 · DOI: 10.1021/nl902701b · Source: PubMed

3 AUTHORS, INCLUDING:

Wenshan Cai
Stanford University
18 PUBLICATIONS **2,134** CITATIONS
SEE PROFILE

Mark L Brongersma
Stanford University
272 PUBLICATIONS **12,120** CITATIONS
SEE PROFILE

NANO LETTERS

2009
Vol. 9, No. 12
4403-4411

Compact, High-Speed and Power-Efficient Electrooptic Plasmonic Modulators

Wenshan Cai, Justin S. White, and Mark L. Brongersma*

Geballe Laboratory for Advanced Materials, Stanford University, 476 Lomita Mall, Stanford, California 94305

Received August 19, 2009; Revised Manuscript Received October 5, 2009

ABSTRACT

CMOS compatible electrooptic plasmonic modulators are slated to be key components in chip-scale photonic circuits. In this work, we investigate detailed design and optimization protocols for electrooptic plasmonic modulators that are suitable for free-space coupling and on-chip integration. The metallic structures in the proposed devices offer simultaneous electric and optical functions. The resonance-enhanced nonlinear interaction and submicrometer-footprint of these devices meet the stringent requirements for future CMOS modulators, allowing for high-speed operation (>100 GHz) with a decent modulation depth (>3 dB) and moderate insertion loss (<3 dB) at a very low swing voltage (~1 V) and power dissipation (~1 fJ/bit). The realization of the proposed structures appears feasible with current materials and lithographic techniques.

The need for nanoscale optical devices is keenly felt as photonic circuits become increasingly prevalent in chip-based communication and signal-processing systems. Recent advances in plasmonics have revealed the great potential of metallic nanostructures to bridge the length-scale mismatch between diffraction-limited dielectric optical systems and nanoscale on-chip electronics.[1−3] As such, plasmonic devices with a subwavelength footprint could play a pivotal role in efforts to seamlessly integrate electronics and photonics on a single Si platform. A range of micrometer-scale passive plasmonic elements have been reported, including basic components such as mirrors,[4] lenses,[5] waveguides[6] as well as functional devices like interferometers,[7,8] splitters,[9] resonators,[10] antennas,[11] and many more. Active plasmonic devices with an externally controlled response are critically important to the successful introduction of plasmonics for on-chip applications. For example, several plasmonic emitters have been recently demonstrated, which can serve as nanoscale light sources for on-chip optical links.[12−14] On the receiving end of such optical communication channels, plasmon-enhanced detectors have shown their strong potential for ultrafast, low-noise and power efficient photodetection.[15−18] A central element in an optical interconnection scheme, an electrooptic plasmonic modulator, is of particular interest, especially considering the fact that some of the most promising Si compatible modulator approaches run into challenges with the weak nonlinear optical effects in Si (e.g., free carrier dispersion) that exhibit poor scaling characteristics.[19−21] If a compact, silicon-compatible electrooptic plasmonic modulator with high-speed and low power consumption as well as reasonable throughput and modulation depth could be designed, it would dramatically impact the development of viable optical interconnect solutions for on-chip applications.

Although the adoption of plasmonic modulators in photonic nanocircuits is a rather novel concept, electrooptic modulation of light based on surface plasmon phenomena was first proposed and demonstrated over two decades ago.[22−25] Most of these early works employed metal-coated prisms in an attenuated total reflection (ATR) geometry to couple a free space light beam to surface plasmon-polaritons (SPPs).[26] For metal films coated with active materials, the light-SPP coupling efficiency and thus the reflected beam intensity can be modulated electrically. Such ATR-based modulation schemes cannot be easily transferred to today's photonic circuits for a number of reasons. First, the geometrical size of these modulators has to be macroscopically large, since conventional optics components like prisms are involved in these setups. Second, the applied voltages in these modulators were too high for integrated photonic circuits; a voltage on the order of 100 V was typically needed to produce useful signal modulation.

In recent years, dynamic control over SPP propagation properties has been realized at the micrometer-scale using a range of approaches. Most of the devices rely on a manipulation of the refractive index of the dielectric layer adjacent to the metal surface. As the propagation of SPPs is critically dependent on this material parameter, modulation can be

* To whom correspondence should be addressed. E-mail: brongersma@stanford.edu. Tel: (650) 736-2152. Fax: (650) 736-1984.

10.1021/nl902701b CCC: $40.75
Published on Web 10/14/2009

easily be attained by affecting the propagation behavior. Pioneering studies on long-range SPP modulators based on thermooptic effects have revealed two key advantages conferred by plasmonics,[27,28] namely the ability to perform simultaneous electric and optical functions in the same structure and the high field confinement near the metal surface. Such electronic control over SPPs has also been demonstrated in other systems consisting of metallic nanostructures and active dielectrics. Examples include the combination of metallic slit or hole arrays with liquid crystals[29] and interfering slit-pairs situated on electrooptically active substrates like barium titanate.[30] Another noticeable example is the recently developed metal-oxide-silicon field effect plasmonic modulator, called a "plasMOSter", which employs the interference between a photonic mode and a plasmonic mode simultaneously supported in the structure.[31] In addition to electrooptic plasmonic modulators, dynamic manipulation of SPPs using other mechanisms have also been studied, including magnetooptic effect,[32] acousto-optic effect,[33] and all optical modulation.[34,35]

Electrooptic materials used in current modulators typically exhibit a quite weak nonlinear interaction with light and as a result modulation schemes tend to need high applied voltages and long interaction channels. To mitigate such constraints, in this paper we turn to resonance-based structures where light-matter interactions can be substantially boosted by engineering high field confinement and enhancement. In nonplasmonic modulators, resonant effects have been successfully used to improve performance.[19−21] In addition to such resonant effects, we will use metal−dielectric−metal (MDM) plasmonic waveguide structures that allow for deep subwavelength optical modes, resulting in compact devices suitable for dense integration.[6] When a nonlinear switching medium is used for the dielectric, a small voltage differential applied to the metals produces high electric fields in the nonlinear medium, resulting in strong switching effects. Recent simulations have aimed to point out several unique advantages of this geometry for optical switching applications by introducing materials with switchable gain or absorption properties.[36,37] Here, we propose and simulate two practical new designs for electrooptic plasmonic modulators that aim to meet the stringent requirements set forth by the electronics industry. One design is for free-space coupling and the other enables integration with conventional waveguides. We show that efficient plasmonic modulation with a 3 dB modulation depth along with modest power attenuation (<3 dB) is possible in a compact device size (small capacitance) with the use of a low swing voltage (1 V) and power consumption. These modulators feature a number of improvements over previous designs and can meet or even exceed the stringent requirements on materials, modulation speed (>40 Gb/s), and energy-efficiency (10 fJ/bit) that will be needed in future chips.

Plasmonic Modulators Employing Free-Space Coupling. We start our design from the simplest prototype of a plasmonic resonator, a two-dimensional slit in a planar metallic slab. In later parts of the paper, we will progressively reinforce and complicate this basic geometry, aiming at producing more efficient structures for plasmonic modulation. The schematic of a metallic slab with an infinitely extended through-slit is shown in Figure 1a. The width and depth of the slit are denoted as w and d, respectively. To reflect the realistic case in nanofabrication processes, we assume that the structure is placed on a transparent substrate with a refractive index n_s, and the slit is filled with a dielectric medium with an index n_d. The slit region is later to be occupied by active materials so that we can realize dynamic control. A plane wave is incident upon the structure from the metal side with its electric field polarized perpendicular to the direction of the slit. Such a state of polarization is necessary to excite the field-symmetric gap plasmon mode propagating through the metallic slit.[38]

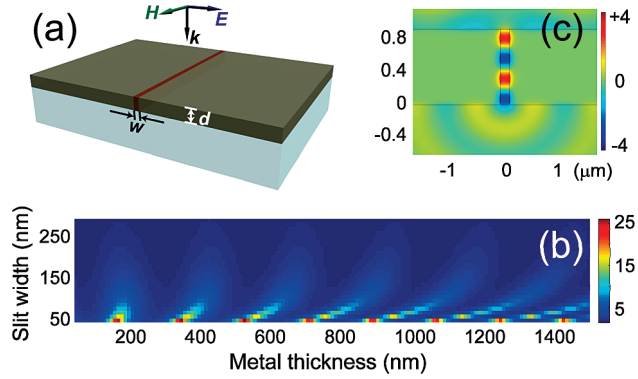

Figure 1. Resonant plasmonic structure consisting of a nanoslit through a metal slab. (a) Schematic view of a nanoslit resonator in a silver slab, along with the operational state of polarization. (b) Normalized energy density within a top-illuminated slit as functions of the slit dimensions. (c) The magnetic field distribution around a top-illuminated slit for a specific resonance condition with $w = 80$ nm and $d_4 = 830$ nm. All fields are normalized to the incident wave.

The slit along with the two interfaces at its ends forms a Fabry−Pérot type resonator for the propagating SPPs in the nanogap, and the resonance condition (multiples of 2π phase pickup for one roundtrip) is critically dependent on the geometrical and material parameters pertinent to the microcavity.[16] Throughout this work we focus our designs on a wavelength of $\lambda_0 = 850$ nm, although these structures and guidelines are generally applicable to all other visible and near-infrared wavelengths as well. To explore the resonant properties of the structure shown in Figure 1a, we perform full-wave finite-element simulations in the frequency domain using a commercial numerical package COMSOL Multiphysics. In our simulations, the permittivity of silver is taken from well accepted experimental data in ref 39 which is $\varepsilon_m = -35.6 + 0.5i$ at the wavelength $\lambda_0 = 850$ nm. The indices of refraction for the glass substrate and the $d \times w$ slit region are set to be $n_s = 1.45$ and $n_d = 1.5$, respectively. A two-dimensional scan of the parameter space (d, w) results in a surface plot for the normalized energy density within the slit, as shown in Figure 1b.

From Figure 1b, we can observe several salient features, which are all explainable within a Fabry−Pérot resonator framework. For a given slit width, there are a series of resonances corresponding to different slab thickness. We

assign the metal thickness d_m for the m-th order of resonance in the cavity. The thickness series d_m is strictly periodic with the separation between adjacent resonances $(d_{m+1} - d_m)$ being half of the gap plasmon wavelength $\lambda_p/2 = \pi/k_p$. The propagation constant k_p for the gap plasmon can be evaluated using the dispersion relation of the plasmon mode[40]

$$\tanh\left(\sqrt{k_p^2 - \varepsilon_d k_0^2}\cdot w/2\right) = -\left(\sqrt{k_p^2 - \varepsilon_m k_0^2}/\sqrt{k_p^2 - \varepsilon_d k_0^2}\right)\cdot(\varepsilon_d/\varepsilon_m)$$

where $k_0 = 2\pi/\lambda_0$ is the vacuum wavevector, and $\varepsilon_d = n_d^2$ is the dielectric constant of the slit medium. The plasmon wavelength λ_p shrinks as the slit width w decreases and the overlap of the plasmon-mode with the metal increases; this directly results in a smaller separation between d_{m+1} and d_m. The propagation of the SPPs in the slit can also be characterized by the mode index $n_p = \lambda_0/\lambda_p$, which gradually approaches the value of n_d with increased slit width. In our case with $w = 80$ nm, the propagation parameters for the gap plasmons are $n_p = 1.91$ and $\lambda_p = 440$ nm. Therefore adjacent resonance thicknesses of the metallic slab are separated by approximately 220 nm. Intriguingly, the thickness d_1 for the very first resonance is smaller than $\lambda_p/2$, a fact related to the additional reflection phase shifts from the two ends of the nanoslit.[41,42] To illustrate the resonance behavior, in Figure 1c we plot the field mapping around the slit at a specific resonance with $w = 80$ nm and $d_4 = 830$ nm. It is interesting to note that although the MDM mode in the slit is intrinsically lossy, both the energy density inside and the transmittance through the slit simultaneously reach their local maxima when the plasmonic resonance condition is fulfilled. Consequently, we can expect a strong light-matter interaction together with a good power throughput from such a structure when used as an active plasmonic device. For example, the resonance shown in Figure 1c gives rise to a time-averaged energy density of about 8 times as large as that of the incident plane wave, and the power passing through the exit of the slit is about 3 times more than the light directly impinging upon the slit area.

In the next part, we seek to further enhance the energy density and power throughput of the metallic slit by adding an extra coupling mechanism. It has been known for years that subwavelength apertures with periodic corrugations in metallic films can support extraordinary transmittance of light, owing to the excitation of SPPs in such systems.[43−45] Here we combine the field confinement arising from a resonant single slit and the antenna-like effect of a grating structure carved into the upper surface of the metal slab. The proposed structure is depicted in Figure 2a. The periodic grooves surrounding the central slit are characterized by three geometrical parameters, the groove width w_g, the groove depth d_g, and the periodicity of the grating p_g. Similar to the previous case, the system is illuminated at normal incidence by a plane wave with transverse magnetic (TM) polarization (magnetic field component parallel to the slit). In such a structure there are two mechanisms that contribute to the simultaneously enhanced confinement and transmittance of light, the Fabry−Pérot resonance supported by the slit and the Bragg grating resonance associated with the periodic array of grooves.

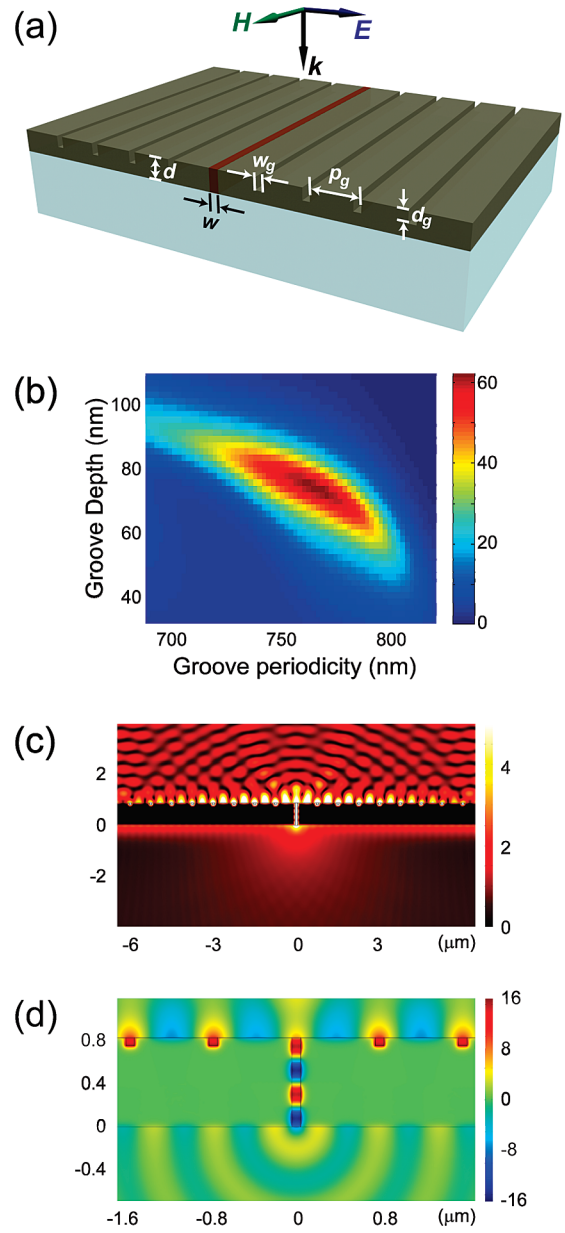

Figure 2. Enhanced transmission through a nanoslit in a metallic film employing grating and slit resonances. (a) Schematic view of the nanoslit resonator surrounded by periodic corrugations. (b) Optimization of power transmission through the slit by using the groove periodicity p_g and depth d_g as free parameters. Other preset parameters include $\lambda_0 = 850$ nm and $w_g = w = 80$ nm. (c) Field mapping for the magnitude of the magnetic field in an optimized structure with the fourth resonance. Note that the field around the central region of the structure is out of the scale bar. (d) Zoomed view for the magnetic field distribution around the central slit when all geometrical parameters are optimized.

The optimized slit parameters are identical to those in the bare slit case, as illustrated in Figure 1b. For the groove parameters, we take the groove width equal to the slit width, that is, $w_g = w = 80$ nm. Next, a two-dimensional scan of the (p_g, d_g) parameter space was performed to locate the optimal values for p_g and d_g. In simulations, we restrict the number of grooves to be 8 on each side of the central slit.

The deviation resulting from this constrained groove number is trivial as compared to the case of infinite gratings. The center-to-center separation between the slit and its closest groove is set to be the same as the groove periodicity p_g. The result of the optimization process is shown in Figure 2b. At the operating wavelength of $\lambda_0 = 850$ nm, the obtained optimal values are $p_g = 766$ nm and $d_g = 72$ nm.

In Figure 2c, we show the magnitude of the magnetic field distribution in an optimized structure, and Figure 2d is a zoomed view for the magnetic field distribution around the central slit. Simulations indicate that the time-averaged energy density inside the central slit can reach about 160 times the value of the incident wave, and the power transmittance is enhanced by an additional 20 times compared to the bare slit case. In other words, the periodic corrugations offer an antenna effect that allows for an effective collection cross-section of ~ 5 μm for an 80 nm wide nanoslit. Such a pronounced enhancement paves the way for efficient light-matter interaction in the proposed structure, which can be used for various types of active plasmonic devices.

To investigate the potential performance of the proposed structure when used as a plasmonic modulator, we assume that the refractive index of the slit medium n_d can be controlled by an externally applied voltage, which results in a change $\Delta n'$ or $\Delta n''$ in either the real or the imaginary part of n_d, respectively. The feasibility of such electronic tuning of n_d in existing materials will be discussed in detail in a later section of this paper. The modulation performance is quantitatively characterized by the modulation depth $M = (I_{ON} - I_{OFF})/I_{ON}$, where I_{ON} and I_{OFF} denote the power flow through the nanoslit in the on and off states, respectively. Figure 3 shows the modulation depth of the device as a function of the changes in the real and imaginary parts of the refractive index within the slit, respectively. In each panel of Figure 3 we plot $M(\Delta n/n)$ for a series of devices with well-defined slab thicknesses at which the Fabry−Pérot resonance condition is met, as indicated by Figure 1b. These devices support resonances of an increasingly high order. For the same change in the slit index, a thicker slab that supports a higher order resonance is favorable in terms of the modulation performance as it provides a larger interaction length between the SPPs and the active material in the slit. For example, when a fourth order resonance is exploited in a $d_4 = 830$ nm thick slab, a change $\Delta n''/n = 0.02$ is required to bring the device from a high transmission on state to a low transmission off state with a modulation depth of 50% (3 dB). In addition, the transmittance in the on state is about 60 as normalized by the light power directly impinging upon the slit area, a quite impressive value considering the sub-100 nm size of the nanoslit. We note that the sensitivity of the modulated output to the change Δn can be further improved by using a narrower slit at the expense of a reduced power transmittance through the structure. The improved performance results from the increased SPP reflection amplitude at the slit terminations, as a consequence of a higher effective mode index and an increased mismatch between the SPP in the slit and the free space modes in the surrounding media.

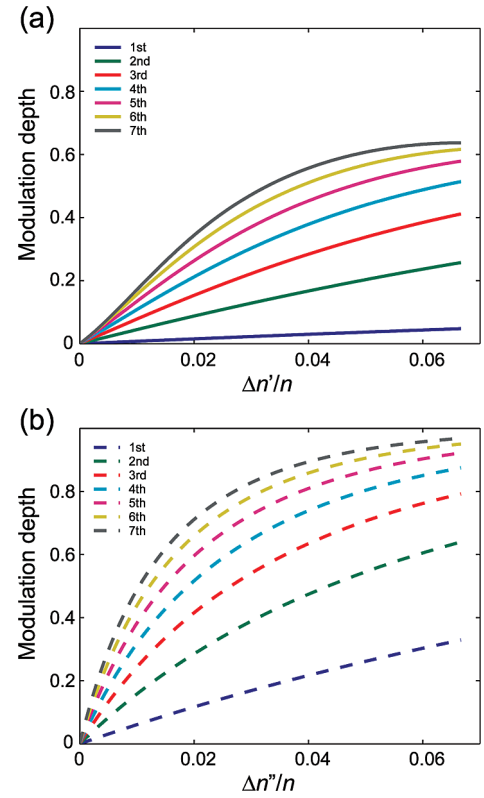

Figure 3. Modulation performance of the plasmonic modulator based on an optimized structure with active materials embedded in a metallic nanoslit surrounded by periodic corrugations. (a,b) The modulation depth of the device as a function of changes in the real and imaginary parts of the refractive index within the slit, respectively. Different orders of resonance correspond to a series of slab thicknesses where Fabry−Pérot resonances in the slit are supported, as indicated by Figure 1b.

Waveguide-Coupled Plasmonic Modulators. In this section, we consider a plasmonic modulator based on an in-plane, MDM waveguide. The MDM plasmonic mode is identical to the gap plasmon in a metallic nanoslit presented in the previous part. Such modes are known to exhibit a high mode confinement along with reasonable propagation length on the order of tens of micrometers, depending on the dielectric layer thickness t for a fixed material combination.[6,46] A schematic view of a MDM modulator is illustrated in Figure 4a, where the resonator is formed by a section of the MDM waveguide with length L together with a pair of rectangular stubs with size $d_s \times w_s$ that can serve as SPP mirrors. To enable a fair comparison between the modulation performance of different designs, we choose the geometrical and material parameters of the MDM modulator similar to those of the slit-based structure, the dielectric layer between two silver slabs is assumed to have a thickness $t = 80$ nm and a refractive index $n_d = 1.5$, and the analysis is carried out for a target wavelength of $\lambda_0 = 850$ nm. As compared to the free-space coupling scheme, the proposed cavity in the MDM waveguide offers several immediately obvious advantages. First, in the in-plane MDM waveguide structure the end mirrors of the Fabry−Pérot resonator can be engineered by optimizing the geometry of the stubs, while the "mirrors" in the slit-based resonator have relatively weak reflectivity as they are formed by the low-contrast interfaces

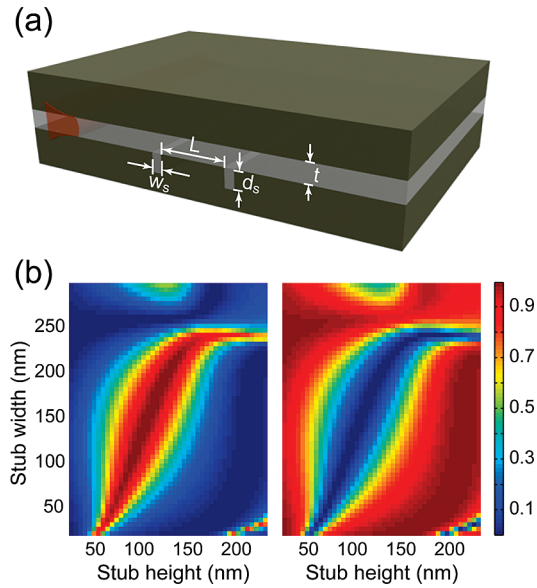

Figure 4. (a) Schematic view of a metal-dielectric-metal waveguide with a pair of stubs in one of the metal slabs. (b) Reflection and transmission intensities of a single stub in a MDM waveguide as functions of stub dimensions.

at the ends of the slit. Second, the in-plane MDM waveguide only supports a single SPP mode for which strong interference effects can be realized between SPPs propagating down the waveguide and SPPs (re)emerging from the stubs, without detrimental coupling to other modes.[6,38,47] Finally, a plasmonic modulator based on a MDM waveguide has a great potential for on-chip integration with conventional dielectric waveguides, a feature necessary for future photonic nanocircuits.

To build a strong Fabry−Pérot resonator into a MDM waveguide, we first optimize its "end mirrors" by choosing the approximate dimensions of the nanostubs. Full-wave simulations result in the reflection and transmission of a single stub in a MDM waveguide as functions of stub dimensions (d_s, w_s), as shown in Figure 4b. The maximum possible reflectance R from a single stub is about 0.985 along with a minimum T of less than 0.001. In an ideal, lossless Fabry−Pérot cavity with a high Q factor, the reflectance R from each end mirror should approach unity, as the finesse of the resonance is proportional to $R/(1 - R)^2$. In our case, however, the highest possible R is not suitable for energy build-up in the cavity, because an MDM plasmonic waveguide is intrinsically lossy. Consequently, if stubs with extremely low T are used to construct the resonator, the energy dissipation within a long effective path ($L_{eff} \sim Q\lambda/2\pi$) would counteract the expected energy buildup and lead to a low intracavity field. Evidently there is a trade off to be made between a number of factors, including the Q factor, the energy enhancement, and the transmittance through the whole structure. For a lossy Fabry−Pérot resonator with a loss factor V per transit ($V = 1$ for the lossless case), the energy density ρ in the cavity is proportional to $(1 - R^2)/(1 - RV)^2$.[48] By setting $\partial\rho/\partial R = 0$ we find that the best light-matter interaction in the cavity occurs when $R = V$. It is straightforward to estimate V for our cavity, which is composed of

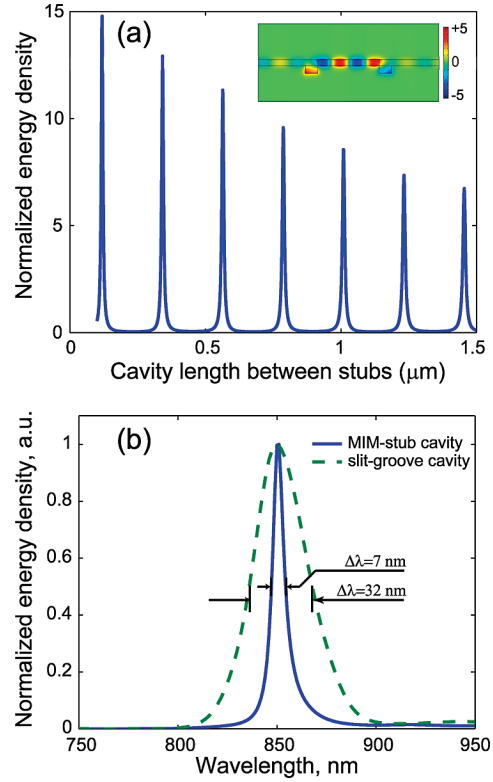

Figure 5. (a) Resonant cavity lengths for a MDM waveguide section with a pair of optimized stubs. Inset: distribution of normalized magnetic field in a fourth order resonator with $L_4 = 790$ nm. (b) Spectral width comparison between the resonance in a MDM-stub cavity and that of a slit-groove cavity.

optical losses in the stub and the cavity. From Figure 4b, we derive that the absorbed fraction of an SPP wave incident on a stub is $A_s = 1 - R - T \approx 0.01$ and largely constant near the optimum stub geometry. To determine the optical losses in traversing the cavity, we use the analytical solution for the gap mode, $k_p = (1.9 + 0.003i)k_0$ and consider a submicrometer cavity length of $L \approx 800$ nm. This gives a propagation loss $A_L = 1 - \exp(-2\mathrm{Im}(k_p)L)$ of about 3% per transit. As a result, we can obtain maximum field enhancement in the resonator when the stub reflectance is made equal to $R = V = 1 - A_s - A_L \approx 0.96$. For any modulator, one needs to find a good compromise between the modulation depth and the transmission through the structure. We choose to reduce the value of R by a few percent in order to achieve a better overall transmission, because the transmittance through the entire MDM-stub cavity $T_{tot} = (1 - R)^2V/(1 - RV)^2$ falls monotonically as R increases. Considering all these factors, we choose the following optimized values for the properties of a single stub: (d_s, w_s) = (95 nm, 160 nm), $R = 0.91$, and $T = 0.08$.

Once the dimensions of the stubs are optimized, we can vary the cavity length L to locate the Fabry−Pérot resonances of different orders. The result is plotted in Figure 5a. Similar to the slit-based resonator, the length series L_m is strictly periodic with the separation between adjacent resonances ($L_{m+1} - L_m$) being half of the gap plasmon wavelength $\lambda_p/2$. As an example, the inset of Figure 5a shows the distribution of normalized magnetic field for a resonator with a length

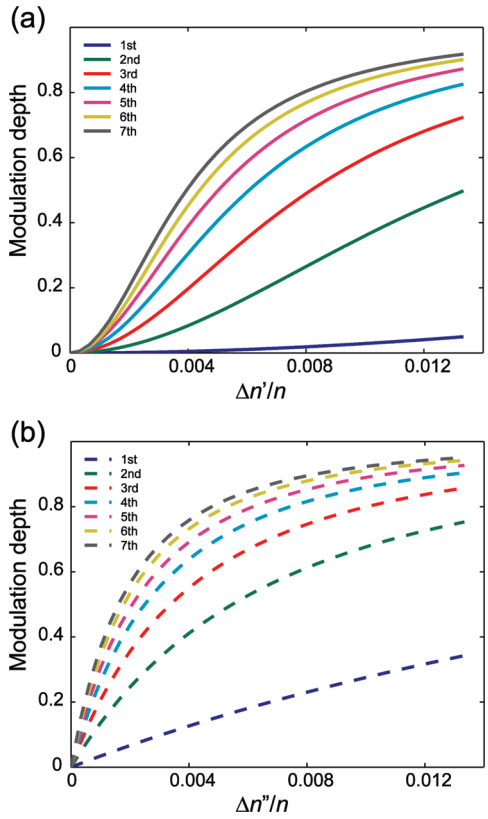

Figure 6. Modulation performance of the plasmonic modulator based on an MDM section with a pair of optimized stubs. (a,b) The modulation depth of the device as a function of changes in the real and imaginary parts of the refractive index within the cavity, respectively. Different orders of resonance correspond to a series of MDM lengths for which Fabry−Pérot resonances in the MDM waveguide are supported, as indicated by Figure 5a.

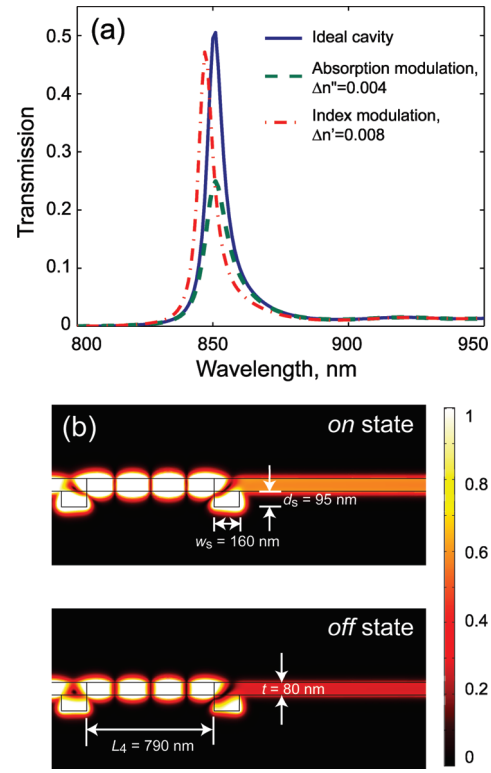

Figure 7. (a) Transmission spectra of the MDM-stub cavity for the on state, the off state with absorption modulation, and the off state with refractive index modulation. (b) Normalized magnetic field mapping for the on state and the off state with 3 dB absorption modulation.

$L_4 = 790$ nm, supporting a fourth order resonance. Comparing Figure 5a to Figure 1b, we see that the resonance in a MDM-stub cavity is much stronger than that of a slit-based structure, thanks to the flexibility of customizing the "mirror" properties when nanostubs are utilized. This feature is better illustrated in the frequency domain, as shown in Figure 5b. In this figure, we compare the spectral width of the two types of cavities of the same order. We see that the full width at half-maximum (FWHM) of a MDM-stub cavity is $\Delta\lambda \approx 7$ nm, which is in good consistency with the analytical estimation of $\Delta\lambda = \lambda_0^2|\ln(RV)|/2\pi n_p L$ from classical resonator theory. This bandwidth implies a cavity Q factor ($Q = \lambda/\Delta\lambda$) of over 100. In contrast to this, the slit-groove structure exhibits a FWHM that is approximately 5 times as large, and the Q factor is much lower than that of the MDM-stub cavity. The strong resonance in the MDM-stub cavity suggests a significant sensitivity to the change of dielectric constant when the structure is used as a plasmonic modulator.

Similar to the last part of the previous section, now we investigate the potential performance of a plasmonic modulator based on the MDM-stub structure. We introduce a change $\Delta n'$ or $\Delta n''$ in either the real or the imaginary part of the refractive index for the dielectric material inside the $L \times t$ cavity region. Figure 6a,b shows the modulation depth M of the device for different resonance orders as functions of $\Delta n'/n$ and $\Delta n''/n$, respectively. Compared with the $M(\Delta n/n)$ dependence for the slit-groove modulator shown in Figure 3, the required change of Δn in MDM-based structure is significantly reduced, owing to the strong resonance and thus the enhanced light-matter interaction in the MDM-stub cavity. Quantitatively, the change in $\Delta n'$ or $\Delta n''$ required for a similar modulation is about 5 times smaller than that of a slit-groove structure, consistent with the spectral width and Q factor comparisons as we have shown in Figure 5b.

Figure 6 shows that for a similar modulation depth at a fixed wavelength of interest, the modulation can be realized by tuning either the real or the imaginary part of the active medium in the cavity region. For example, when the fourth order resonator ($L_4 = 790$ nm) is used, a 3 dB modulation depth ($M = 0.5$) can be obtained by introducing either a $\Delta n'' = 0.004$ in the imaginary part or a $\Delta n' = 0.008$ in the real part of n_d. These two types of modulation mechanism act differently on the transmission through the resonant structure. Increases in the imaginary part $\Delta n''$ raise the power dissipation in the cavity medium, and consequently, the overall strength of the Fabry−Pérot resonance is suppressed. Alternatively, modulation of the real part of n_d shifts the central wavelength of the resonance, as the optical path per transit is changed. The scenario is illustrated in Figure 7a, where the transmission spectra of the MDM-stub cavity for three cases, the on state, the off state with absorption modulation, and the off state with refractive index modulation, are obtained from simulations. To further illustrate the field distribution in the device, in Figure 7b we show the normalized magnetic field maps for the on state and the off

state with a 3 dB absorption modulation. Despite the lossy nature of both the metallic waveguide and the stub-based end-mirrors, the power transmittance after the entire Fabry−Pérot resonator is over 50%, quite impressive for a metallic cavity-modulator.

Materials Considerations. Up to this point, our modulator analysis was carried out based on some hypothetical active media whose optical properties (in terms of the real and imaginary parts of refractive index) can be tuned by an externally applied voltage. For example, according to the modulation depth plot in Figure 6, a 3 dB modulation depth in a fourth order MDM-stub cavity requires either $\Delta n'' = 0.004$ in the imaginary part or $\Delta n' = 0.008$ in the real part of the refractive index inside the cavity. The feasibility of the proposed devices is critically dependent on the availability of such active materials, and we address this issue next.

A number of schemes can be used to control the flow of light electrically. Two of the most prominent ones are the electroabsorption (EA) effect, where the absorption coefficient of a material can be altered by an applied electric field, and the electrorefractive effect (sometimes simply referred to as the "electrooptic effect"), where an applied electric field changes the real part of the refractive index of the material. Note that many materials exhibit both effects simultaneously at the same wavelength, because the refractive index and the absorption coefficient are interrelated, as governed by the Kramers−Kronig relations. Useful EA effects can occur in bulk semiconductors, namely the Franz−Keldysh effect, which is used in most commercial EA modulators, and in some quantum confined structures known as the quantum-confined Stark effect (QCSE), which is a much stronger EA effect than seen in bulk semiconductors.[49] The required change $\Delta n'' = 0.004$ in our previous example corresponds to a change of $\Delta\alpha = 600\ \mathrm{cm}^{-1}$, a value achievable with both types of EA effects. For example, the Franz−Keldysh effect in III−V semiconductors gives rise to a typical absorption coefficient change of $\Delta\alpha \approx 4 \times 10^{-4} F^2$ $\mu\mathrm{mV}^{-2}$,[50] where F represents the applied electric field. Therefore the required $\Delta\alpha = 600\ \mathrm{cm}^{-1}$ is possible through the Franz−Keldysh effect with less than 1 V applied across the metallic nanogap of 80 nm. This shows ones of the key benefits of using plasmonic waveguides that support deep-subwavelength optical modes. QCSE can serve as an even better mechanism for providing the change of $\Delta\alpha$, because the obtained $\Delta\alpha/F^2$ via QCSE in quantum wells can be an order of magnitude larger than that of bulk Franz−Keldysh effect. Moreover, strong QCSE within the silicon−germanium system was experimentally realized recently,[51] which makes possible a CMOS compatible plasmonic modulator if similar quantum structures were to be used as active media in our designs. When semiconductor-based active materials are used, the modulation performance of the slit-groove modulator can be enhanced due to a stronger cavity resonance resulting from a sharper contrast between the refractive index of the plasmon mode and that of the free space. The use of high-index cavity materials also helps to make more compact modulators, as the cavity length can be reduced due to a shrunk surface plasmon-polariton wavelength.

As for the electronic control over the real part of refractive index by electrorefractive effects, linear electrooptic effects (Pockels effect) in crystals and semiconductors are routinely used in most interference-based electrooptic modulators. Electrooptic effects in polymers can also be used in our plasmonic modulator designs. For example, a nonlinear coefficient r_{33} of over 200 pm/V has been obtained in several types of nonlinear chromophores.[52] If such molecules are introduced to the proposed nanostructures, an applied voltage of 2 V is sufficient to provide a $\Delta n' = r_{33} n_0^3 F/2$ of over 0.008 as required in our previous discussion. We also note that there are several ways to increase the modulation sensitivity of the device at the expense of the overall transmittance. For the absorption modulation, our numerical work shows that if the stub depth is increased by 5 nm, the required $\Delta n''$ can be reduced by about 30% while the transmittance of the device in the on state is decreased by a similar relative fraction. This is because we can approach the maximum field-enhancement condition ($R = V \approx 0.96$) by increasing the depth of the stubs. As for the index-modulation scheme, we can move the operation condition slightly away from the center position of the Fabry−Pérot resonance. In this scenario, the operational point is located on the steep slope of the resonance spectrum, where a higher sensitivity is expected as compared to that of the "flat" resonance peak. Moreover, an asymmetric MDM-stub cavity has the potential of providing better modulation performance due to the extra flexibility in engineering the resonator.

Integration of Plasmonic Modulators on a Si Chip. In this part, we consider the coupling efficiency of the MDM-stub structure for on-chip integration. Recent theoretical investigations show that a properly designed coupler can provide a coupling efficiency of over 90% between a silicon waveguide and an MDM plasmonic channel.[53] The efficient coupling between an MDM waveguide and a standard silicon waveguide has also been experimentally confirmed.[54] Considering the overall transmittance of over 50% in the proposed modulator, as indicated in Figure 7a, the total insertion loss can be controlled well close to 3 dB when both ends of the MDM-stub modulator are connected to silicon waveguides on the same photonic circuit.

We note that although all examples used thus far are designed for a wavelength of $\lambda_0 = 850$ nm, the implementation protocol is very general and can be easily applied to other operational frequencies. For example, based on the same MDM waveguide we can build a plasmonic modulator for the telecommunication wavelength of $\lambda_0 = 1.5\ \mu$m with modulation performance similar to the features shown in Figure 6. For this scaled-up modulator, we found optimized stub dimensions of $(d_s, w_s) = (200, 230$ nm) and a channel length between the two stubs of $L = 1.48\ \mu$m. We also note that besides silver, other noble metals can also be used for the design, especially for near-infrared and longer wavelengths where the metal permittivities are large and negative. Considering the recently developed highly efficient active materials based on QCSE in Ge/SiGe quantum structures, a CMOS compatible plasmonic modulator for on-chip optical interconnect is not beyond the reach of current technologies.

We also note that when connected with a dielectric waveguide, the lateral size of the modulator would be the same as that of the dielectric strip, which is on the order of 1 μm. Such a modification does not induce noticeable deterioration to the device performance, unless the lateral size shrinks down to the deep subwavelength regime (a few tens of nanometers).

Modulation Speed and Power Consumption. One of the most important strengths of plasmonic modulators is the projected speeds and power consumption, which directly benefit from the small modulator size. The modulation bandwidth is proportional to $1/RC$ where R is loading resistance and C is the capacitance of the structure. In our proposed structures, the cavity length is smaller than 1 μm, so the unit gap capacitance is roughly 1 fF/μm, assuming gaps of 80 nm and dielectric constants of $\varepsilon_r \approx 10$. For practical applications, the MDM-stub modulator need to be coupled to a conventional dielectric waveguide, thus the dimension along the magnetic field direction would be the same as the width of a silicon waveguide, which is on the order of 1 μm. Given a typical loading resistance of $R = 50$ Ω, the RC time constant of the proposed modulator is about 50 fs, and the estimated rise time of a step response is $\sim$100 fs. Consequently, we expect a RC-limited modulation bandwidth on the order of terahertz, far exceeding the bandwidth requirement in the state-of-the-art on-chip optical systems. Therefore the modulation speed of the designed plasmonic modulator is primarily determined by the material response rather than the RC limitations. The mechanisms proposed to be used in our designs, including the electroabsorption effects in bulk or quantum-confined semiconductors and the electrorefractive effect in polymers are all in principle suitable for operating speeds of 100 GHz or higher.

The low capacitance of the structure also gives rise to a highly desirable power efficiency. A future chip-scale optical link requires extremely low power consumption, ideally on the order of $\sim$10 fJ/bit.[55] Such an energy target is not readily achievable in conventional all-dielectric modulators. The plasmonic modulator proposed in this work offers considerable potential to meet this demand, thanks to the small size together with the resonance-enhanced light-matter interaction. The power dissipation of an optical modulator can be estimated as $P = CV_\pi^2 f/2$, where V_π is the voltage swing and f represents the operating frequency. Given V_π of $\sim$1 V and unit capacitance of $\sim$1 fF/μm as shown in previous discussions, the projected power consumption in the device is on the order of 1 fJ/bit, perfectly suitable for on-chip communication and signal processing.

Conclusions. Plasmonic nanostructures are slated to play a significant role in future, on-chip optical interconnection schemes, owning to their ability to simultaneously carry both electric signals and optical modes with subwavelength dimensions. In this work we presented a detailed design protocol for electrically addressable plasmonic modulators that are suitable for silicon-compatible chip-scale applications. The proposed devices are very compact and utilize a Fabry−Pérot resonance to substantially enhance the nonlinear interaction between the surface plasmon-polariton modes and active materials. For a 3 dB modulation depth, the device requires a very modest change of $\Delta n'' = 0.004$ or $\Delta n' = 0.008$ in the cavity index. Such changes are well within the reach of a variety of available electrooptic effects. The estimated swing voltage of $\sim$1 V and capacitance of $\sim$1 fF promise ultrahigh-speed operation at very low power dissipation, ideally suited for chipscale optical communication and signal processing systems. This investigation could redefine the way in which electrooptic plasmonic modulators will be designed in the future.

Acknowledgment. We gratefully acknowledge financial support from the Intel Corporation for this research. We would also like to thank Bruce Block from Intel for many fruitful discussions on the topics of this paper.

References

(1) Zia, R.; Schuller, J. A.; Chandran, A.; Brongersma, M. L. *Mater. Today* **2006**, *9* (7−8), 20–27.
(2) Ebbesen, T. W.; Genet, C.; Bozhevolnyi, S. I. *Phys. Today* **2008**, *61* (5), 44–50.
(3) Atwater, H. A. *Sci. Am.* **2007**, *296* (4), 56–63.
(4) Ditlbacher, H.; Krenn, J. R.; Schider, G.; Leitner, A.; Aussenegg, F. R. *Appl. Phys. Lett.* **2002**, *81* (10), 1762–1764.
(5) Liu, Z. W.; Steele, J. M.; Srituravanich, W.; Pikus, Y.; Sun, C.; Zhang, X. *Nano Lett.* **2005**, *5* (9), 1726–1729.
(6) Zia, R.; Selker, M. D.; Catrysse, P. B.; Brongersma, M. L. *J. Opt. Soc. Am. A* **2004**, *21* (12), 2442–2446.
(7) Schouten, H. F.; Kuzmin, N.; Dubois, G.; Visser, T. D.; Gbur, G.; Alkemade, P. F. A.; Blok, H.; Hooft, G. W.; Lenstra, D.; Eliel, E. R. *Phys. Rev. Lett.* **2005**, *94* (5), 053901.
(8) Zia, R.; Brongersma, M. L. *Nat. Nanotechnol.* **2007**, *2* (7), 426–429.
(9) Bozhevolnyi, S. I.; Volkov, V. S.; Devaux, E.; Laluet, J. Y.; Ebbesen, T. W. *Nature* **2006**, *440* (7083), 508–511.
(10) Min, B. K.; Ostby, E.; Sorger, V.; Ulin-Avila, E.; Yang, L.; Zhang, X.; Vahala, K. *Nature* **2009**, *457* (7228), 455–458.
(11) Muhlschlegel, P.; Eisler, H. J.; Martin, O. J. F.; Hecht, B.; Pohl, D. W. *Science* **2005**, *308* (5728), 1607–1609.
(12) Koller, D. M.; Hohenau, A.; Ditlbacher, H.; Galler, N.; Reil, F.; Aussenegg, F. R.; Leitner, A.; List, E. J. W.; Krenn, J. R. *Nat. Photonics* **2008**, *2* (11), 684–687.
(13) Jun, Y. C.; Kekatpure, R. D.; White, J. S.; Brongersma, M. L. *Phys. Rev. B* **2008**, *78* (15), 153111.
(14) Hryciw, A.; Jun, Y. C.; Brongersma, M. L. *Opt. Express* **2009**, *17* (1), 185–192.
(15) Ishi, T.; Fujikata, J.; Makita, K.; Baba, T.; Ohashi, K. *Jpn. J. Appl. Phys., Part 2* **2005**, *44* (12−15), L364–L366.
(16) White, J. S.; Veronis, G.; Yu, Z. F.; Barnard, E. S.; Chandran, A.; Fan, S. H.; Brongersma, M. L. *Opt. Lett.* **2009**, *34* (5), 686–688.
(17) Tang, L.; Kocabas, S. E.; Latif, S.; Okyay, A. K.; Ly-Gagnon, D. S.; Saraswat, K. C.; Miller, D. A. B. *Nat. Photonics* **2008**, *2* (4), 226–229.
(18) Neutens, P.; Van Dorpe, P.; De Vlaminck, I.; Lagae, L.; Borghs, G. *Nat. Photonics* **2009**, *3* (5), 283–286.
(19) Lipson, M. *Nanotechnology* **2004**, *15* (10), S622–S627.
(20) Liu, A. S.; Jones, R.; Liao, L.; Samara-Rubio, D.; Rubin, D.; Cohen, O.; Nicolaescu, R.; Paniccia, M. *Nature* **2004**, *427* (6975), 615–618.
(21) Kekatpure, R. D.; Brongersma, M. L.; Shenoy, R. S. *Opt. Lett.* **2005**, *30* (16), 2149–2151.
(22) Sincerbox, G. T.; Gordon, J. C. *Appl. Opt.* **1981**, *20* (8), 1491–1494.
(23) Schildkraut, J. S. *Appl. Opt.* **1988**, *27* (21), 4587–4590.
(24) Solgaard, O.; Ho, F.; Thackara, J. I.; Bloom, D. M. *Appl. Phys. Lett.* **1992**, *61* (21), 2500–2502.
(25) Jung, C.; Yee, S.; Kuhn, K. *Appl. Opt.* **1995**, *34* (6), 946–949.
(26) Raether, H. *Surface Plasmons*; Springer-Verlag: New York, 1988.
(27) Nikolajsen, T.; Leosson, K.; Bozhevolnyi, S. I. *Appl. Phys. Lett.* **2004**, *85* (24), 5833–5835.
(28) Nikolajsen, T.; Leosson, K.; Bozhevolnyi, S. I. *Opt. Commun.* **2005**, *244* (1−6), 455–459.
(29) Dickson, W.; Wurtz, G. A.; Evans, P. R.; Pollard, R. J.; Zayats, A. V. *Nano Lett.* **2008**, *8* (1), 281–286.
(30) Dicken, M. J.; Sweatlock, L. A.; Pacifici, D.; Lezec, H. J.; Bhattacharya, K.; Atwater, H. A. *Nano Lett.* **2008**, *8* (11), 4048–4052.
(31) Dionne, J. A.; Diest, K.; Sweatlock, L. A.; Atwater, H. A. *Nano Lett.* **2009**, *9* (2), 897–902.

(32) Chau, K. J.; Irvine, S. E.; Elezzabi, A. Y. *IEEE J. Quantum Electron.* **2004**, *40* (5), 571–579.
(33) Gerard, D.; Laude, V.; Sadani, B.; Khelif, A.; Van Labeke, D.; Guizal, B. *Phys. Rev. B* **2007**, *76* (23), 235427.
(34) Pacifici, D.; Lezec, H. J.; Atwater, H. A. *Nat. Photonics* **2007**, *1* (7), 402–406.
(35) Pala, R. A.; Shimizu, K. T.; Melosh, N. A.; Brongersma, M. L. *Nano Lett.* **2008**, *8* (5), 1506–1510.
(36) Yu, Z.; Veronis, G.; Fan, S. H.; Brongersma, M. L. *Appl. Phys. Lett.* **2008**, *92* (4), 041117.
(37) Min, C.; Veronis, G. *Opt. Express* **2009**, *17* (13), 10757–10766.
(38) Economou, E. N. *Phys. Rev.* **1969**, *182* (2), 539–554.
(39) Johnson, P. B.; Christy, R. W. *Phys. Rev. B* **1972**, *6* (12), 4370–4379.
(40) Prade, B.; Vinet, J. Y.; Mysyrowicz, A. *Phys. Rev. B* **1991**, *44* (24), 13556–13572.
(41) Gordon, R. *Phys. Rev. B* **2006**, *73* (15), 153405.
(42) Bozhevolnyi, S. I.; Sondergaard, T. *Opt. Express* **2007**, *15* (17), 10869–10877.
(43) Ebbesen, T. W.; Lezec, H. J.; Ghaemi, H. F.; Thio, T.; Wolff, P. A. *Nature* **1998**, *391* (6668), 667–669.
(44) Lezec, H. J.; Degiron, A.; Devaux, E.; Linke, R. A.; Martin-Moreno, L.; Garcia-Vidal, F. J.; Ebbesen, T. W. *Science* **2002**, *297* (5582), 820–822.
(45) Garcia-Vidal, F. J.; Lezec, H. J.; Ebbesen, T. W.; Martin-Moreno, L. *Phys. Rev. Lett.* **2003**, *90* (21), 213901.
(46) Shin, H.; Yanik, M. F.; Fan, S. H.; Zia, R.; Brongersma, M. L. *Appl. Phys. Lett.* **2004**, *84* (22), 4421–4423.
(47) Liu, J. S. Q.; White, J. S.; Fan, S. H.; Brongersma, M. L. *Opt. Express* **2009**, *17* (20), 17837–17848.
(48) Hodgson, N.; Weber, H. *Laser Resonators and Beam Propagation*; Springer: New York, 2005.
(49) Miller, D. A. B.; Chemla, D. S.; Damen, T. C.; Gossard, A. C.; Wiegmann, W.; Wood, T. H.; Burrus, C. A. *Phys. Rev. B* **1985**, *32* (2), 1043–1060.
(50) Chin, M. K. *IEEE Photonics Technol. Lett.* **1995**, *7* (3), 309–311.
(51) Kuo, Y. H.; Lee, Y. K.; Ge, Y. S.; Ren, S.; Roth, J. E.; Kamins, T. I.; Miller, D. A. B.; Harris, J. S. *Nature* **2005**, *437* (7063), 1334–1336.
(52) Kim, T. D.; Kang, J. W.; Luo, J. D.; Jang, S. H.; Ka, J. W.; Tucker, N.; Benedict, J. B.; Dalton, L. R.; Gray, T.; Overney, R. M.; Park, D. H.; Herman, W. N.; Jen, A. K. Y. *J. Am. Chem. Soc.* **2007**, *129* (3), 488–489.
(53) Veronis, G.; Fan, S. H. *Opt. Express* **2007**, *15* (3), 1211–1221.
(54) Chen, L.; Shakya, J.; Lipson, M. *Opt. Lett.* **2006**, *31* (14), 2133–2135.
(55) Miller, D. A. B. *Proc. IEEE* **2009**, *97* (7), 1166–1185.

NL902701B